Time-varying characteristics of bridges under the passage of vehicles using synchroextracting transform

Jiantao Li[1a], Xinqun Zhu*[a], Siu-seong Law[b] and Bijan Samali[c]

[a] *School of Civil and Environmental Engineering, University of Technology Sydney, Broadway, NSW 2007, Australia.* [1]*Email: jiantao.li@student.uts.edu.au*
**Corresponding author: xinqun.zhu@uts.edu.au*
[b] *School of Civil Engineering, Chongqing University. Email: siu-seong.law@connect.polyu.hk*
[c] *School of Computing, Engineering and Mathematics, Western Sydney University, Penrith, NSW 2751, Australia. E-mail: b.samali@westernsydney.edu.au*

Abstract

The vehicle and bridge responses in a vehicle-bridge interaction (VBI) system have been widely studied with some aiming at the bridge health monitoring. The extraction of bridge modal frequencies from bridge or vehicle responses was mostly conducted with the assumption of an invariant vehicle and bridge system and/or the responses are stationary during the interaction. This assumption may be appropriate when the vehicle mass is negligible compared with the bridge mass. The vehicle and bridge frequencies are time-varying in practice during the VBI process and these time-varying characteristics are potential indicators for bridge condition assessment. This paper presents a new method to extract the time-varying characteristics of the bridge under the passage of vehicles. A time-frequency (TF) analysis method, the synchroextracting transform, is adopted for the purpose. It is a post-processing procedure with short-time Fourier transform to improve the TF resolution on the time-varying features of the signal. The instantaneous frequency of mono-components related to the vehicle and bridge frequencies can then be extracted from the time-frequency representation of the responses. Numerical investigation is conducted to study the effect of measurement noise, vehicle properties and road surface roughness on the identified results. Laboratory and field tests are also conducted to validate the proposed approach. Results show that the time-varying characteristics are good indicators for bridge condition assessment.

Keywords: vehicle-bridge interaction, frequency variation, time-frequency analysis, synchroextracting transform,

1. Introduction

Research in last decade has witnessed the extensive study on vehicle-bridge interaction (VBI) for the purpose of bridge structural condition assessment (SHM) (Law and Zhu, 2004; Chen et al., 2009; Kim et al., 2014; Nguyen, 2015; Khan et al., 2016). The VBI-based approach allows the target bridge to be monitored or assessed under operating conditions (Zhu and Law, 2015). The output-only approaches make use of the vibration responses from an instrumented bridge, i.e. stochastic subspace identification, frequency domain decomposition and random decrement technique, etc., to extract the structural properties. White noise input to the structure is commonly assumed. However, the VBI system is time-variant with the operational variations of traffic excitation on the structure. The use of vehicle responses for indirect bridge monitoring also draws great research attention due to its low cost and convenience. Yang et al. (2004) pioneered the work of indirect bridge frequency identification using vehicle responses by spectrum analysis. González et al. (2012) identified the bridge damping using a moving instrumented vehicle. The vehicle response has also been used for bridge mode shape identification (Yang et al., 2014; Malekjafarian and OBrien, 2017). Most of the above methods assumed non-varying frequencies of the vehicle and structure, which is approximately relevant when the VBI effect is negligible. For the case where the vehicle mass is not small compared to the bridge mass, the frequency variation of the system due to the interaction cannot be ignored as noted in several experimental investigations (Farrar et al., 1997; Zhang et al., 2002; Kim and Lynch, 2012).

Several reports have also been published on the frequency variation in the vehicle-bridge interaction system. Li et al. (2003) theoretically studied the natural frequency of railway girder bridges under vehicular load. The bridge frequency was found varying periodically with the passage of the vehicle. Kim et al. (2003) experimentally studied the effect of vehicle weight on the bridge natural frequencies under traffic-induced excitation. A change of 5.4% was noted in the natural frequencies of a short span bridge with a 3.8% mass ratio between that of a vehicle and the bridge super-structure. Law and Zhu (2004) studied the effect of crack in bridge structures on the instantaneous frequency (IF) under moving vehicular loads. The frequency changes due to a moving mass and a moving oscillator were compared. The changes were found sensitive to the weight of vehicle and the frequency ratio between the vehicle and bridge. Yang et al. (2013) presented a theoretical framework with closed-form solutions on the frequency variation of the VBI system considering only the first bridge vibration mode. Both the vehicle and bridge frequencies varied roughly in the form of half-sinewave with respect to the vehicle location. A larger vehicle/bridge mass ratio yielded larger frequency deviations. When the vehicle/bridge frequency ratio is close to unity, the vehicle and bridge frequencies (Yang et al., 2013) deviated drastically from their natural values. Chang et al. (2014) studied the variability of bridge frequency due to a vehicle parked on top theoretically and experimentally. Cantero et al. (2017) conducted field tests on the evolution of bridge modal properties including the bridge frequencies and vibration modes during the passage of

a truck. They also assessed the non-stationary and non-linear features of the vehicle responses experimentally from a scaled vehicle-bridge interaction test bed (Cantero et al., 2019). Despite of the many studies mentioned above, the non-stationary properties of bridge vibration under a passing vehicle is still not fully explored (Xiao et al., 2017).

Time-frequency (TF) analysis is an effective tool for the analysis of nonstationary signals. The classical linear methods, such as the short time Fourier transform (STFT) and wavelet transform can expand a one-dimensional time-series signal onto the two-dimensional TF plane for further signal decomposition. However, the time-frequency representations (TFRs) generated are often blurry, and it is difficult to provide a precise time-frequency description on a time-varying signal. The Wigner-Ville distribution gives optimal energy concentration for mono-component linear frequency modulation, but it produces undesirable cross-terms for non-linear frequency modulated or multi-component signals (Boashash and Aïssa-El-Bey, 2018). Advanced methods have been developed since to improve the performance of conventional methods in the analysis of time varying signal, e.g. synchrosqueezing transform (SST) (Daubechies et al., 2011) and high-order SST (Wang et al., 2014). Recently, a TF analysis technique called synchroextracting transform (SET) has been proposed (Yu et al., 2017). It improves the energy concentration of the TFRs by retaining only the time-frequency information most related to the time-varying features of the signal. It outperforms the STFT in this aspect. The measured response from the vehicle of the VBI system is multicomponent which is related to the vehicle frequency, bridge frequency and the road surface roughness. The bridge response is a superposition of several vibration modes. Decompose the multicomponent signal into mono-component mode is an effective way to study the behaviours of individual component. Each mono-component mode in a well-separated multicomponent signal can be extracted from the TFR (Meignen et al., 2016) based on which the IF can be estimated (Thakur and Wu, 2011). Hilbert-Huang transform (HHT) (Huang et al. 1998) and wavelet transform (WT) have been used for the time-frequency analysis of nonstationary dynamic responses. Wang et al. (2012) compared the HHT and WT for TF analysis of a coupled VBI bridge system with breathing cracks. Cantero et al. (2017) and Yang et al. (2019) used continuous wavelet transform (CWT) to study the nonstationary features of the bridge under vehicle excitations. The signal can be decomposed into intrinsic mode functions (IMFs) by the HHT and the IFs of the system are obtained from IMFs. The WT can be used to decompose the signal into different frequency band components, but only the energy distribution with time can be obtained. Wavelet Synchrosqueezing transform (WSST) has been proposed as a time-frequency signal analysis method to improve the resolutions in the time and frequency domains (Thakur, 2013).

This study further explores the variability in the vehicle and bridge frequencies due to the VBI with the TF analysis using the SET. The effects of vehicle properties, moving speed, road

surface roughness and measurement noise on the frequency variation are studied. Numerical and experimental validation of the proposed approach are also reported.

The rest of this paper is organized as follows. The VBI model is firstly introduced followed by description of the TF analysis method based on SET and the mono-component extraction. Numerical and experimental studies are then presented with conclusions drawn.

2. Vehicle-bridge interaction model

A VBI model is shown in Figure 1. The vehicle is modelled as a quarter car and the bridge as a simply-supported beam with length L. The vehicle is assumed to move along the bridge deck at a constant velocity v. Parameters m_v, k_v and c_v are the vehicle mass, stiffness and damping, respectively. The equation of motion of the discretized vehicle and the bridge system can be expressed as

$$m_v\ddot{d}_v(t) + c_v\dot{d}_v(t) + k_v d_v(t) = F(t) \tag{1}$$

$$\mathbf{M}_b\ddot{\mathbf{d}}_b(t) + \mathbf{C}_b\dot{\mathbf{d}}_b(t) + \mathbf{K}_b\mathbf{d}_b(t) = \mathbf{H}_c(t)P_{int}(t) \tag{2}$$

where d_v and $\mathbf{d}_b$ denotes the vertical displacement of the vehicle and bridge respectively. $\mathbf{M}_b$, $\mathbf{C}_b$, $\mathbf{K}_b$ are the mass, damping and stiffness matrices of the bridge, respectively. $F(t)$ is the force on the vehicle system and $P_{int}(t)$ is the interacting force between the vehicle and bridge. $\mathbf{H}_c(t) = \{0, 0 \dots, \boldsymbol{H}_i(t), \dots, 0\}^T$ is a function of time and $\boldsymbol{H}_i(t)$ is the vector of shape function in the *ith* element on which the moving vehicle is located at time instant *t*, and it can be expressed as $\boldsymbol{H}_i(t) = \{1 - 3\xi^2 + 2\xi, (\xi - 2\xi^2 + \xi^3)l_e, 3\xi^2 - 2\xi^3, (-\xi^2 + \xi^3)l_e\}$, with $\xi = (x(t) - x_i)/l_e$, $x_i = (i - 1)l_e$ where l_e is the length of the element (Zhu et al,. 2018).

The equation of motion of the coupled VBI system can be obtained as

$$\begin{bmatrix} \mathbf{M}_b & m_v\mathbf{H}_c \\ \mathbf{0} & m_v \end{bmatrix} \begin{Bmatrix} \ddot{\mathbf{d}}_b \\ \ddot{d}_v \end{Bmatrix} + \begin{bmatrix} \mathbf{C}_b & \mathbf{0} \\ -c_v\mathbf{H}_c^T & c_v \end{bmatrix} \begin{Bmatrix} \dot{\mathbf{d}}_b \\ \dot{d}_v \end{Bmatrix} + \begin{bmatrix} \mathbf{K}_b & \mathbf{0} \\ -k_v\mathbf{H}_c^T - c_v\dot{\mathbf{H}}_c^T & k_v \end{bmatrix} \begin{Bmatrix} \mathbf{d}_b \\ d_v \end{Bmatrix} = \begin{Bmatrix} \mathbf{H}_c m_v g \\ k_v r(x) + c_v v r'(x) \end{Bmatrix} \tag{3}$$

where $r(x)$ is the profile of surface roughness of the bridge deck. The system matrices of the coupled interaction system in Eq. (3) are noted time-dependent according to the location of the interacting force and the frequencies of the system are time-varying. Yang et al. (2013) derived the vehicle and bridge instantaneous frequencies, i.e. ω_v and ω_b considering only the first bridge vibration mode of the Euler-Bernoulli beam and neglecting the damping effect and surface roughness as:

For $\omega_{v0} > \omega_{b0}$

$$\omega_v^2 = \frac{\omega_{v0}^2}{2} + \frac{\omega_{b0}^2}{2} + \frac{m_v\omega_{v0}^2}{\rho L}\sin^2\left(\frac{\pi x_c}{L}\right) + \sqrt{\left(\frac{\omega_{v0}^2}{2} + \frac{\omega_{b0}^2}{2} + \frac{m_v\omega_{v0}^2}{\rho L}\sin^2\left(\frac{\pi x_c}{L}\right)\right)^2 - \omega_{v0}^2\omega_{b0}^2} \quad (4a)$$

$$\omega_b^2 = \frac{\omega_{v0}^2}{2} + \frac{\omega_{b0}^2}{2} + \frac{m_v\omega_{v0}^2}{\rho L}\sin^2\left(\frac{\pi x_c}{L}\right) - \sqrt{\left(\frac{\omega_{v0}^2}{2} + \frac{\omega_{b0}^2}{2} + \frac{m_v\omega_{v0}^2}{\rho L}\sin^2\left(\frac{\pi x_c}{L}\right)\right)^2 - \omega_{v0}^2\omega_{b0}^2} \quad (4b)$$

For $\omega_{v0} < \omega_{b0}$

$$\omega_v^2 = \frac{\omega_{v0}^2}{2} + \frac{\omega_{b0}^2}{2} + \frac{m_v\omega_{v0}^2}{\rho L}\sin^2\left(\frac{\pi x_c}{L}\right) - \sqrt{\left(\frac{\omega_{v0}^2}{2} + \frac{\omega_{b0}^2}{2} + \frac{m_v\omega_{v0}^2}{\rho L}\sin^2\left(\frac{\pi x_c}{L}\right)\right)^2 - \omega_{v0}^2\omega_{b0}^2} \quad (4c)$$

$$\omega_b^2 = \frac{\omega_{v0}^2}{2} + \frac{\omega_{b0}^2}{2} + \frac{m_v\omega_{v0}^2}{\rho L}\sin^2\left(\frac{\pi x_c}{L}\right) + \sqrt{\left(\frac{\omega_{v0}^2}{2} + \frac{\omega_{b0}^2}{2} + \frac{m_v\omega_{v0}^2}{\rho L}\sin^2\left(\frac{\pi x_c}{L}\right)\right)^2 - \omega_{v0}^2\omega_{b0}^2} \quad (4d)$$

where ω_{v0} and ω_{b0} are the original vehicle and bridge natural frequencies respectively, and x_c is the location of the vehicle on the deck. It has been reported (Yang et al., 2013) that the largest deviation of the vehicle and bridge frequencies occur when the vehicle is close to mid-span of the deck.

3. Extraction of time-varying characteristics of the VBI system with SET

3.1 The SET theory

The STFT of a signal $s(t)$ with a real and even window $h(t)$ can be written as

$$X_w(t,\omega) = \int_{-\infty}^{\infty} s(\tau)h(\tau - t)e^{-i\omega\tau}\, d\tau \quad (5)$$

where $h(\tau - t)$ denotes the moving window and $s(\tau)$ is the measured signal. The STFT expands a 1-D time-series signal onto the 2-D TF plane for a display of the time-frequency information. For a purely harmonic signal $s_h(t) = Ae^{i\omega_0 t}$ with frequency ω_0 and invariant amplitude A, its STFT can be expressed as

$$X_h(t,\omega) = A * \hat{h}(\omega - \omega_0) * e^{i\omega_0 t} \quad (6)$$

where $\hat{h}(\omega - \omega_0)$ is the Fourier transform (FT) of the window function. In the time and frequency domains, the bandwidth of the window function leads to an energy-smeared spectrogram. It is therefore difficult to characterize the time-varying feature of a signal precisely. In this study, the IF trajectory (Yu et al., 2017) is adopted to improve the resolution of the time-frequency representation in the framework of SST. To obtain the IF of the STFT, the derivative of $X_h(t,\omega)$ with respect to time *t* is calculated as

$$\partial_t X_h(t,\omega) = X_h(t,\omega) * i * \omega_0 \quad (7)$$

A 2-D IF $\omega_0(t,\omega)$ for any (t,ω) and $X_h(t,\omega) \neq 0$ can be obtained from

$$\omega_0(t,\omega) = -i * \frac{\partial_t X_h(t,\omega)}{X_h(t,\omega)} \tag{8}$$

Yu et al. (2017) generated a novel TFR using only the TF coefficient in the IF trajectory $\omega = \omega_0$ similar to SST as

$$Te(t,\omega) = X_h(t,\omega) * \delta(\omega - \omega_0(t,\omega)) \tag{9}$$

where

$$\delta\big(\omega - \omega_0(t,\omega)\big) = \begin{cases} 1, & \omega = \omega_0 \\ 0, & \omega \neq \omega_0 \end{cases} \tag{10}$$

This post-processing procedure extracts the TF coefficient of $X_h(t,\omega)$ only in the IF trajectory $\omega = \omega_0$, and the rest of the TF coefficients are ignored. In this study, only the largest TF coefficient is used to generate a novel TFR to have a minimum noise effect on the TF result.

3.2 Time-frequency representation of response of the VBI system

The response of the VBI system can be expressed as

$$s(t) = \sum_{k=1}^{n} s_k(t) = \sum_{k=1}^{n} A_k(t) * e^{i\varphi_k(t)} \tag{11}$$

where $\varphi_k(t)$ and its first-order derivative $\varphi'_k(t)$ are the instantaneous phase and the instantaneous frequency of the *kth* component respectively. The STFT of $s(t)$ can be represented by the first-order approximation (Meignen et al. 2016) as

$$X_h(t,\omega) \approx \sum_{k=1}^{n} A_k(t) * \hat{h}(\omega - \varphi'_k(t)) e^{i\varphi_k(t)} \tag{12}$$

For well-separated measured response, the IF of each mode can be estimated from

$$\varphi'(t,\omega) = \sum_{k=1}^{n} \varphi'_k(t) = -i * \frac{\partial_t X_h(t,\omega)}{X_h(t,\omega)} \tag{13}$$

The SET expression can then be written as

$$Te(t,\omega) = X_h(t,\omega) * \delta(\omega - \varphi'(t,\omega)) \tag{14}$$

and the signal can be reconstructed approximately by

$$s(t) \approx \sum_{k=1}^{n} Te\big(t, \varphi'_k(t)\big)/\hat{h}(0) \tag{15}$$

Each mode can then be decomposed with first-order approximation as

$$s_k(t) \approx e\big(t, \varphi'_k(t)\big)/\hat{h}(0) \tag{16}$$

3.3 Time-varying characteristics of the VBI system using ridge detection

A popular multi-ridge detection algorithm (Thakur et al., 2013) is employed to decompose the measured response and to estimate all IF trajectories at the same time. This technique aims at finding the best frequency curve (denoted as $\Omega_i(t)$) in the TFR X_h, which maximizes the energy with a smoothness constraint through a total variation penalization term expressed as

$$\widehat{\Omega} = \underset{\Omega}{\operatorname{argmax}} \int |X_h(t, \Omega(\mathrm{t}))|^2 dt - \lambda \int \left| \frac{d\Omega(\mathrm{t})}{dt} \right|^2 dt \tag{17}$$

where λ controls the importance of the smoothness constraint. For multi-component extraction, this method can be iterated after setting X_h equals to null in the vicinity of the previously detected ridge (Fourer et al., 2017).

3.4 Simply-support beam subjected to white noise excitation

A simply-supported beam subjected to white noise excitation is shown in Figure 2. The physical properties of the beam are: $L = 30m, \rho = 6000\, kg/m$, $EI = 2.5e10Nm^2$ with the damping neglected. White noise excitation is applied at Node 9 vertically and the vertical acceleration response at Node 4 is calculated with the Newmark-β method at 0.01s time interval. The white noise is added to the calculated acceleration response to simulate the polluted measurement as

$$acc_m = acc_{cal} + E_p * N_{oise} * \sigma(acc_{cal}) \tag{18}$$

where acc_{cal} is the calculated acceleration response, $E_p$is the noise level, N_{oise} is a standard normal distribution vector with zero mean and unit variance, and $\sigma(acc_{cal})$ is the standard deviation of the calculated acceleration response.

Five percent white noise is added to the calculated acceleration responses to simulate the measured data. Figure 3 shows the applied force and Figure 4 shows the vertical acceleration response at Node 4 and its response spectrum. Two dominant peaks are found at 3.55Hz and 13.40Hz corresponding to the first two modal frequencies of the beam. The measured data are analysed using STFT and SET with a window length of 2048, and the TFR of the signal is presented in Figures 5(a) and 5(b). Both figures show two straight lines representing the first two modal frequencies of the beam in the time-frequency domain. The solid line in Figure 5(a) indicates a high energy component. The line is noted horizontal indicating the invariability of frequency under given excitation condition. The energy of TFR by SET as shown in Figure 5(b) is noted more concentrated than that by direct STFT in Figure 5(a). Therefore, the SET will be used for the time-frequency analysis in the rest of the paper. The IF trajectories corresponding to the first two bridge vibration modes are given in Figure 6(a) and the TFR of the mono-component modes are presented in Figure 6(b). Both figures exhibit stationary features of the responses.

4. Numerical study on the VBI system

4.1 Time-frequency analysis of vehicle and bridge responses

The VBI system as shown in Figure 1 is studied. The bridge properties are the same as those in Section 3.4 but with the inclusion of bridge damping. Rayleigh damping is assumed with $\mathbf{C}_b=\alpha_1\mathbf{M}_b+\alpha_2\mathbf{K}_b$ and $\alpha_1=0.243$, $\alpha_1=0.0001$, where $\mathbf{M}_b$, $\mathbf{C}_b$ and $\mathbf{K}_b$ are the mass, damping and stiffness matrices of the bridge respectively. A vehicle model with parameters $m_v = 500kg$, $k_v = 2.02e5\ N/m$ and $c_v = 390\ N/m/s$ (Yang et al., 2013) is adopted. The natural frequency of the vehicle is 3.20Hz and the vehicle/bridge mass ratio is 0.003. The bridge deck surface is assumed smooth. The vehicle is assumed moving on a 50m approach road before entering the bridge. The response is obtained by solving the coupled vehicle-bridge interaction equation using Newmark-β method with 500Hz sampling rate. 5% white noise is added to the calculated acceleration according to Eq. (18) to simulate the measurement with the SNR equals to 26. Figure 7(a) shows the bridge response at Node 4 and its spectrum when the vehicle moves at 2m/s. Figure 7(b) shows the vehicle response and its spectrum. The first bridge modal frequency of 3.60Hz can be identified from the bridge and vehicle responses. The responses are further input into the SET to get the time-frequency information with a window length of 2048. The TFRs obtained from the bridge and vehicle responses are presented in Figures 8(a) and 8(b) respectively. The time-frequency information related to the first and second bridge modes can be observed in Figure 8(a). However, only that related to the first mode is noted from the vehicle response in Figure 8(b). Figure 8(c) presents the IF trajectories of different modes without obvious variation in the frequency due to the very small vehicle/bridge mass ratio.

The effects of measurement noise on the time-frequency identification using the proposed method are further studied by considering two additional noise levels, i.e. 10% and 15%. The IF trajectories obtained from the responses are given in Figure 9. It is noted that the TF analysis results are very robust to the measurement noise. Therefore 5% measurement noise is considered in the following numerical studies.

4.2 Effect of vehicle/bridge mass and frequency ratios

The TF characteristics of the VBI system are studied by considering different vehicle parameters. Besides Vehicle 1 adopted in Section 4.1, another three vehicle models (denote as Vehicles 2 to 4) are considered with the vehicle properties listed in Table 1. The vehicle damping $c_v = 390N/m/s$ is the same for all vehicles. The bridge model is same as that in Section 3.4 and the vehicle/bridge mass and frequency ratios are listed in Table 1. Vehicles 1 and 2 have the same frequency ratio 0.9, and their mass ratios are 0.003 and 0.039, respectively. Vehicles 2 and 3 have the same mass ratio 0.039, and their frequency ratios are 0.9 and 0.24 respectively. Vehicle 4 has the frequency ratio

1.07 and the mass ratio 0.019. These vehicle models are used in the simulation to get the corresponding vehicle and bridge responses. The proposed method is used to extract the IFs from the responses.

Figures 8 and 10 show the results with Vehicles 1 and 2. Figure 8(c) shows no clear variation in the frequency because of the negligible small vehicle/bridge mass ratio of 0.003 for Vehicle 1. Similar TF analysis as for Vehicle 1 is conducted for Vehicle 2 which has the vehicle/bridge mass ratio of 0.039, and the IF trajectories extracted from the bridge and vehicle responses from the TFRs are shown in Figures 10(a). The frequencies of the vehicle and bridge are noted varying in roughly a half-sinewave with respect to the location of the moving vehicle. The frequency related to the first bridge mode increases as the vehicle moves toward midspan of the bridge and decreases when moving away from midspan. The vehicle frequency shows an opposite trend. For the second bridge vibration mode, no obvious frequency variation is noted. Therefore, the first bridge vibration mode and vehicle mode are studied further. Theoretical instantaneous frequencies are calculated by solving the eigenvalue problem of the equation of motion of the system. Figure 10(b) compares the results identified from the present analysis procedure and the theoretical analysis (Yang et al., 2013) with good agreement. A comparison of results from Vehicles 1 and 2 shows that there is frequency variation when a heavy vehicle crosses the bridge.

To further study the effect of the vehicle/bridge frequency ratio, the time-frequency analysis on the bridge and vehicle responses gives the IF results for Vehicles 3 and 4 as shown in Figure 11. Vehicle 3 has the same mass ratio as Vehicle 2 but with a frequency ratio of 0.24. The vehicle/bridge mass and frequency ratios for Vehicle 4 are 0.019 and 1.07 respectively. The TF plots for Vehicle 3 in Figure 11(a) do not feature any obvious frequency variation in both TFRs because the vehicle/frequency ratio is much smaller than one although the vehicle/bridge mass ratio is large. In contrast, the case with Vehicle 4 shows clear variation in the vehicle and bridge frequencies as shown in Figure 11(b). These variation of frequencies shows opposite trend with that of Vehicle 2 in Figure 10(b) as the vehicle/bridge frequency ratio for this case is larger than one. The above results are consistent with that in Eq. (4). A comparison of the above results shows that the time-varying characteristics of a vehicle-bridge interaction system are affected by the vehicle/bridge frequency ratio. The frequency change is defined as $\frac{|\omega-\omega_0|}{\omega_0} \times 100\%$. The maxima of the bridge frequency change and vehicle frequency change are calculated from Eq. (4) and they are plotted against the vehicle/bridge mass ratio and frequency ratio in Figures 12(a) and 12(b) respectively. Only the cases of Vehicles 2 and 4 are noted exhibiting prominent changes, i.e. 9.3% and 8.5% for Vehicle 2 and 7.3% and 7.9% for Vehicle 4 respectively in the bridge and vehicle frequencies, while those in Vehicles 1 and 3 are very small. The frequency variation is mainly affected by the vehicle/bridge mass and frequency ratios. When under the passage of the heavy vehicle and with the vehicle/bridge frequency ratio is close to one, the VBI system is approaching

the resonance condition, and both the vehicle and bridge frequencies will have significant deviation around the original natural frequencies. Otherwise, there is no obvious deviation.

4.3 Effect of different measurement points on the bridge

Vertical accelerations collected at three locations, i.e. 3/20, 7/20 and 11/20 of the bridge span from the left support, are analysed to study the effect of different measurement location on the frequency variation. Vehicle 2 is used and 5% measurement noise is included. The extracted IF trajectories of responses at different points are presented in Figure 13. The IF trajectories are noted the same from responses at different measurement points studied.

4.4 Effect of vehicle speed

Vehicle 2 moving at 4m/s is used for this study while other parameters are the same as those for the above cases. The time-frequency analysis results are shown in Figure 14. For different vehicle speeds, similar trend of frequency variation of the system can be observed. However, a higher moving speed means a shorter duration of vehicle-bridge interaction with less measured data for the analysis, and this may reduce the resolution of the TFR. Therefore a lower moving speed of vehicle is recommended to obtain more accurate TFR of the signal from vehicle response.

4.5 Effect of the bridge surface roughness

A smooth bridge deck has been adopted in the above studies while Class A (ISO, 1995) surface roughness is used in this study. Vehicle speed is 2m/s and 5% measurement noise is included. The bridge and vehicle responses in time-frequency domain obtained from SET are shown in Figures 15(a) and 15(b), respectively. The vehicle related frequency is noted more dominant with the effect of road roughness. The bridge related frequency from vehicle response becomes blurred in the time-frequency domain. By using the mode extraction technique in Section 3.2, the extracted components are shown in Figure 16(b), and the results are agreed well with that for smooth bridge surface in Figure 16(a). It can be seen that the TFR related to the bridge vibration mode can be clearly extracted as shown in Figure 16(b).

4.6 Comparison with HHT and WSST

The discussions above on the time-varying characteristics of the VBI system have shown that the SET is an effective tool for the analysis of the nonstationary responses of the system. To further demonstrate the effectiveness and merits of the SET, another two widely used TF analysis techniques, i.e. HHT and WSST, are adopted for comparison of the instantaneous frequencies of the

VBI system. The response of vehicle 2 moving on the smooth bridge deck at 2m/s is used. 10% measurement noise is considered. The identified IF results are given in Figure 17. Figure 17(a) shows the IF trajectory related to the 1st bridge frequency by HHT. It is noted that the HHT cannot identify the vehicle related frequency since it is close to the bridge frequency. The time-varying characteristic cannot be identified directly. Figure 17(b) shows the IF trajectories by WSST and SET. It can be seen that both techniques can obtain the IF trajectories related to the vehicle and bridge frequencies, and the time-varying characteristic of the system can be noted clearly. However, the results obtained from WSST suffer from the edge effects at the beginning and end of the signal. This comparison demonstrates that SET is more suitable for the TF analysis of the VBI system compared to the other two techniques.

5. Laboratory investigation

5.1 TF analysis of the vehicle and bridge responses

A vehicle-bridge model has been fabricated in the laboratory as shown in Figure 18. The bridge model consists of three rectangular steel beams. The one in the middle is the main beam with 6m length and 100mm × 15mm cross-section. It is simply-supported beam with two spans. The first two natural frequencies of the bridge model are 5.68 and 8.48 Hz, respectively obtained by modal test. A leading beam and a trailing beam are sitting in front of and at the rear of the main beam to allow for acceleration and deceleration of the vehicle. The length of these beams is 3m. Vehicle model with two axles and 5kg weight is built for the study with a 4kg mass block placed on top of the vehicle. The first natural frequency of the vehicle is 32.15Hz. The frequency ratio between the first vehicle and bridge natural frequencies is 5.66. A U-shaped aluminium section is glued to the top surface along the middle line of the beam as direction guide for the vehicle. The model vehicle is pulled along the guide by a string wound around the drive wheel of an electric motor. BeanDevice AX-3D wireless accelerometers are used to measure the dynamic response of the vehicle during its passage over the bridge, and they are installed above the axles as shown in Figure 19.

The vehicle is moving at approximately 0.61m/s over the main beam. Acceleration responses from above the vehicle front axle and at midpoint of the first span of beam are collected. The signal and the spectra are shown in Figure 20(a). The components in the responses related to the first bridge mode and vehicle mode are extracted. The IF trajectories for the components are given in Figure 20(b). The evolution of the IF trajectory are found similar for the bridge and vehicle responses. The IF trajectory related to the vehicle frequency from the bridge response has more fluctuations compared to that obtained directly from the vehicle response. A comparison with the IF trajectories in Figure 10 shows that the deviation in Figure 20(b) is minimal. This is mainly due to

the large frequency ratio between the first vehicle and bridge natural frequencies (5.66) which is much larger than one. The frequency ratio in Figure 10(b) is 0.90 which facilitates a resonance condition leading to larger deviations in the IF.

5.2 The case with an extra mass added to midpoint of first span of the beam

A 5kg mass is hung at midspan of the first span of the beam to simulate a variation of the beam model, as shown in Figure 21. The vehicle moves over the bridge at the same speed as in last study. The TFA results of the bridge and vehicle responses are presented in Figures 22(a) and 22(b), respectively. The IF trajectory for the vehicle mode does not change much with the addition of the extra mass. The result related to the first bridge vibration mode obtained from the bridge response shows that the IF trajectory is generally lower than the one without the additional mass. The result from the vehicle response shows that the IF trajectory becomes higher with the additional mass.

6. Field study with a cable-stay bridge

A long-term monitoring system has been installed on a cable-stayed bridge as shown in Figure 23(a). The structure carries a single lane highway with a length of 46m and a width of 5m. The bridge connects the South and North campuses of the Western Sydney University. Figure 23(b) shows that there are two continuous spans in the bridge deck and the structural mast is the internal support which is very close to the south entrance of the bridge. There are 24 accelerometers on the bridge deck, and a strain gauge is installed on each cable supporting the deck. Figures 23(b) and 23(c) show the sensor locations. A data acquisition system continuously records the data from sensors with a sampling rate of 600Hz. The vehicle-induced responses of the bridge will be analysed for this study.

6.1 The case with different traffic conditions on the bridge

Responses from sensor A10 under three different traffic conditions are measured. Case 1 has no vehicle on the bridge. Case 2 has one vehicle moving on the bridge from North to South and Case 3 has one vehicle moving on the bridge from South to North. There is a roundabout at the southern entrance of the bridge. The acceleration responses and the spectra are shown in Figure 24.

When there is no traffic on the bridge, only the first bridge frequency can be identified in the response spectrum. For the other two cases with moving vehicle on top of the bridge, the higher bridge vibration modes are more prominent due to the vehicular excitations. The TF analysis results of the responses under different traffic conditions are presented in Figure 25. When there is no traffic on the bridge, the IF trajectory of the first bridge vibration mode shows little variation. For the cases with moving vehicle, the IF trajectories corresponding to the bridge vibration modes exhibit large variations. When the vehicle moves from South to North, the frequency changes are

smaller than those when the vehicle moves from North to South. This may be due to a shorter span of 4m at the South entrance of the bridge.

To better understand how the cables respond to the moving vehicle, the strain measurements on four cables at one side of the deck are shown in Figure 26. The strain increases when the vehicle is in its vicinity and decreases when the vehicle moves away. The function of the cables may be simplified as vertical spring supports at the connection points with the deck. The composite effects of the vehicle and cables account for the time-varying behaviors of the bridge frequencies.

6.2 TF analysis results of responses at different locations

Responses measured at different locations with the vehicle moving from North to South are analyzed. Measurements from sensors A6, A10, A14 and A18 along the bridge deck are analyzed for comparison. Similar analysis on the responses from sensors A9, A10, A11 and A12 in the transverse direction is also conducted. The IF trajectories of the first two bridge vibration modes from different responses are shown in Figure 27.

The IF trajectories from sensors A6 and A10 exhibit similar trend for the first two bridge vibration modes and they are larger than those from responses measured at A14 and A18. For the sensors in the transverse direction, the frequency variations obtained from the responses are almost the same for the first bridge vibration mode. However, the variations are different for the second bridge vibration mode but with a similar trend. This may be explained that the second vibration mode consists of a mixture of torsion and bending modes from the operational modal analysis (Sun et al., 2017).

7. Conclusions

The time-varying characteristics of the vehicle-bridge interaction system are studied numerically and experimentally. A time-frequency analysis strategy, synchroextracting transform, is adopted to study the vehicle and bridge responses with improved time-frequency resolution. Component extraction is conducted to obtain the instantaneous frequency related components of the vehicle and bridge as well as the IF trajectories. The effects of vehicle parameters, moving speed, road surface roughness and measurement noise on the instantaneous frequency are numerically investigated.

The instantaneous frequency variation is sensitive to the vehicle/bridge mass ratio. When the vehicle mass is negligible compared to the bridge mass, the frequency of the system is non-varying. Both the vehicle and bridge frequency variations can be observed in the instantaneous frequencies of the responses when the vehicle/bridge mass ratio is large and the vehicle/bridge frequency ratio is close to one. The time-varying characteristics of the vehicle-bridge interaction are

also noted in a VBI system fabricated in the laboratory. Analysis on the bridge responses of an actual cable-stay bridge shows that the instantaneous frequency are affected by the combined effects of moving vehicle and the cables. The time-varying characteristics of the bridge under the passage of vehicles have a big potential for bridge structural health monitoring in practice.

Acknowledgements

This research is supported by research funding of the Australian Research Council Discover Project (DP160103197). The financial aid is gratefully acknowledged. The data from the field bridge is instrumented by DATA61 which is greatly acknowledged.

References

Boashash B and Aïssa-El-Bey A. (2018) Robust multisensor time–frequency signal processing: A tutorial review with illustrations of performance enhancement in selected application areas. *Digital Signal Processing* 77: 153-186.

Cantero D, Hester D and Brownjohn J. (2017) Evolution of bridge frequencies and modes of vibration during truck passage. *Engineering Structures* 152: 452-464.

Cantero D, McGetrick P, Kim CW and O'Brien EJ(2019) Experimental monitoring of bridge frequency evolution during the passage of vehicles with different suspension properties. *Engineering Structures* 187: 209-219.

Chang KC, Kim CW and Borjigin S. (2014) Variability in bridge frequency induced by a parked vehicle. *Smart Structures and Systems* 13: 755-773.

Chen YB, Feng MQ and Tan CA. (2009) Bridge structural condition assessment based on vibration and traffic monitoring. *Journal of Engineering Mechanics ASCE*, 135(8): 747-758.

Daubechies I, Lu JF and Wu HT. (2011) Synchrosqueezed wavelet transforms: An empirical mode decomposition-like tool. *Applied and Computational Harmonic Analysis* 30: 243-261.

Farrar CR, Doebling SW, Cornwell PJ and Straser EG(1997) Variability of modal parameters measured on the alamosa canyon bridge. *Proceedings of SPIE, the International Society for Optical Engineering.* Society of Photo-Optical Instrumentation Engineers, 257-263.

Fourer D, Harmouche J, Schmitt J, Oberlin T, Meigen S, Auger F and Flandrin P. (2017) The ASTRES toolbox for mode extraction of non-stationary multicomponent signals. *Proceedings of EUSIPCO (2017)*: 1170-1174.

González A, O'Brien EJ and McGetrick P. (2012) Identification of damping in a bridge using a moving instrumented vehicle. *Journal of Sound and Vibration* 331: 4115-4131.

Huang NE, Shen Z, Long SR, et al. (1998) The empirical mode decomposition and the Hilbert spectrum for nonlinear and non-stationary time series analysis. *Proceedings of the Royal Society of London. Series A: Mathematical, Physical and Engineering Sciences* 454: 903-995.

ISO 8608 (1995), *Mechanical Vibration–Road Surfaces Profiles–Reporting of Measured Data*. International Organization for Standardization, Switzerland.

Khan SM, Atamturktur S, Chowdhury M and Rahman M. (2016) Integration of structural health monitoring and intelligent transportation systems for bridge condition assessment: current status and future direction. *IEEE Transactions on Intelligent Transportation Systems* 17: 2107-2122.

Kim CW, Isemoto R, McGetrick P, Kawatani M and O'Brien EJ. (2014) Drive-by bridge inspection from three different approaches, *Smart Structures and Systems*, 13(5): 775-796.

Kim CY, Jung DS, Kim NS, Kwon SD and Feng MQ. (2003) Effect of vehicle weight on natural frequencies of bridges measured from traffic-induced vibration. *Earthquake Engineering and Engineering Vibration* 2(1): 109-115.

Kim J and Lynch JP. (2012) Experimental analysis of vehicle–bridge interaction using a wireless monitoring system and a two-stage system identification technique. *Mechanical Systems and Signal Processing* 28: 3-19.

Law SS and Zhu XQ. (2004) Dynamic behavior of damaged concrete bridge structures under moving vehicular loads. *Engineering Structures* 26: 1279-1293.

Li JZ, Su MB and Fan LC. (2003) Natural frequency of railway girder bridges under vehicle loads. *Journal of Bridge Engineering ASCE*, 8(4): 199-203.

Malekjafarian A and O'Brien EJ. (2017) On the use of a passing vehicle for the estimation of bridge mode shapes. *Journal of Sound and Vibration*, 397: 77-91.

Meignen S, Oberlin T, Depalle P, Flandrin P and McLaughlin S. (2016) Adaptive multimode signal reconstruction from time–frequency representations. *Philosophical Transactions of the Royal Society A: Mathematical, Physical and Engineering Sciences* 374(2065): 20150205.

Nguyen KV. (2015) Dynamic analysis of a cracked beam-like bridge subjected to earthquake and moving vehicle. *Advances in Structural Engineering* 18: 75-95.

Sun M, Makki Alamdari M and Kalhori H. (2017) Automated operational modal analysis of a cable-stayed bridge. *Journal of Bridge Engineering ASCE* 22: 05017012.

Thakur G, Brevdo E, Fuckar NS and Wu HT. (2013) The Synchrosqueezing algorithm for time-varying spectral analysis: robustness properties and new paleoclimate applications. *Signal Processing*, 93(5): 1079-1094.

Thakur G and Wu HT. (2011) Synchrosqueezing-based recovery of instantaneous frequency from nonuniform samples. *SIAM Journal on Mathematical Analysis* 43: 2078-2095.

Wang SB, Chen XF, Cai GG, Chen BQ, Li X and He ZJ (2014) Matching Demodulation Transform and SynchroSqueezing in Time-Frequency Analysis. *IEEE Transactions on Signal Processing* 62: 69-84.

Wang WJ, Lu ZR and Liu JK. (2012) Time-frequency analysis of a coupled bridge-vehicle system with breathing cracks. *Interaction and multiscale mechanics* 5: 169-185.

Xiao F, Chen GS, Hulsey JL and Zatar W. (2017) Characterization of non-stationary properties of vehicle–bridge response for structural health monitoring. *Advances in Mechanical Engineering* 9: 1687814017699141.

Yang YB, Cheng MC and Chang KC. (2013) Frequency variation in vehicle–bridge interaction systems. *International Journal of Structural Stability and Dynamics* 13: 1350019.

Yang J, He XH, Zou YF, Zhu XJ and Zhang LH (2019) Time-frequency features of continuous metro bridge under various excitations. *Proceedings of Experimental Vibration Analysis for Civil Engineering Structures (EVACES 2019)*, 5-8 September, Nanjing, Jiangsu, China.

Yang YB, Li YC and Chang KC. (2014) Constructing the mode shapes of a bridge from a passing vehicle: a theoretical study. *Smart Structures and Systems* 13: 797-819.

Yang YB, Lin CW and Yau JD. (2004) Extracting bridge frequencies from the dynamic response of a passing vehicle. *Journal of Sound and Vibration* 272: 471-493.

Yu G, Yu MJ and Xu CY. (2017) Synchroextracting transform. *IEEE Transactions on Industrial Electronics* 64: 8042-8054.

Zhang QW, Fan LC and Yuan WC. (2002) Traffic-induced variability in dynamic properties of cable-stayed bridge. *Earthquake Engineering & Structural Dynamics* 31: 2015-2021.

Zhu XQ and Law SS (2015) Structural health monitoring based on vehicle-bridge interaction: accomplishments and challenges. *Advances in Structural Engineering*, 18(12): 1999-2015.

Zhu XQ, Law SS, Huang L and Zhu SY. (2018) Damage identification of supporting structures with a moving sensory system. *Journal of Sound and Vibration* 415: 111-127.

Table 1 Properties of vehicle models

Vehicle	$k_v\ (N/m)$	$m_v\ (kg)$	$\omega_{v0}\ (Hz)$	Vehicle/bridge mass ratio	Vehicle/bridge frequency ratio
1	2.02e5	500	3.20	0.003	0.90
2	2.82e6	7000	3.20	0.039	0.90
3	2.02e5	7000	0.86	0.039	0.24
4	2.02e6	3500	3.82	0.019	1.07

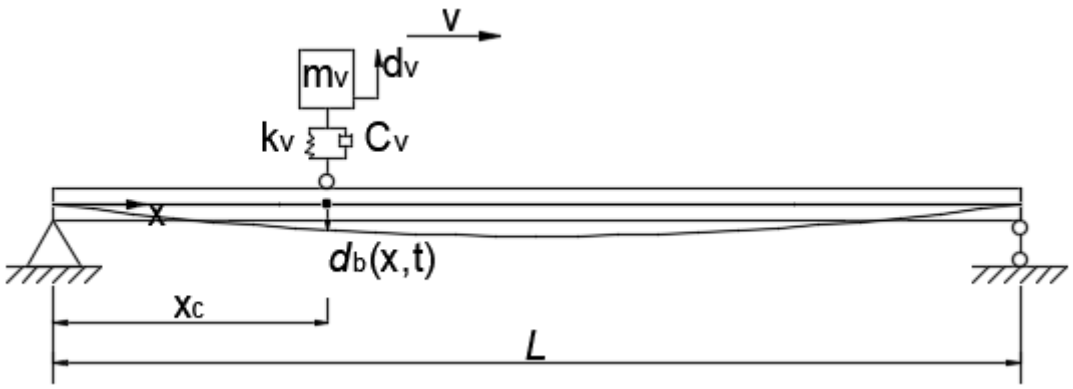

Figure 1 Vehicle-bridge interaction model

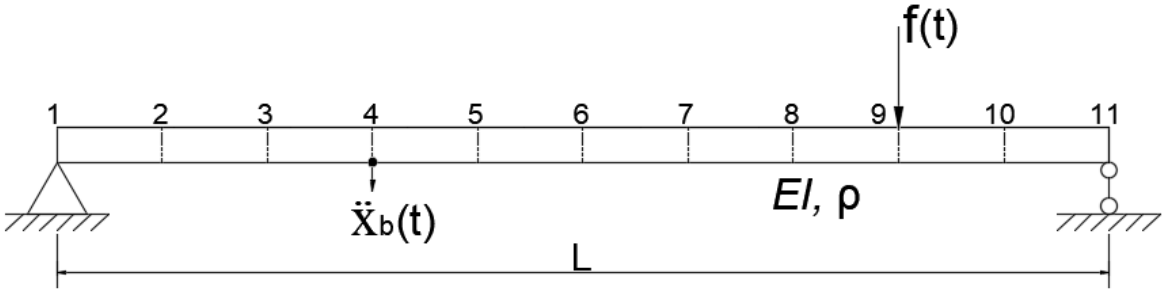

Figure 2 A simply-supported beam under random force

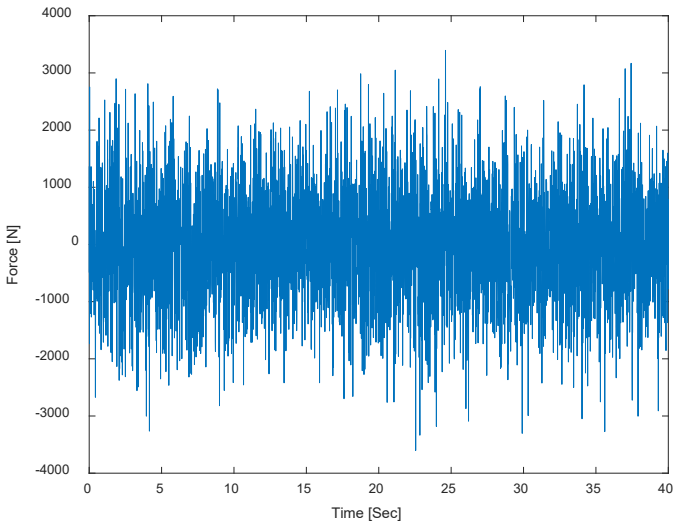

Figure 3 Applied force to the beam model

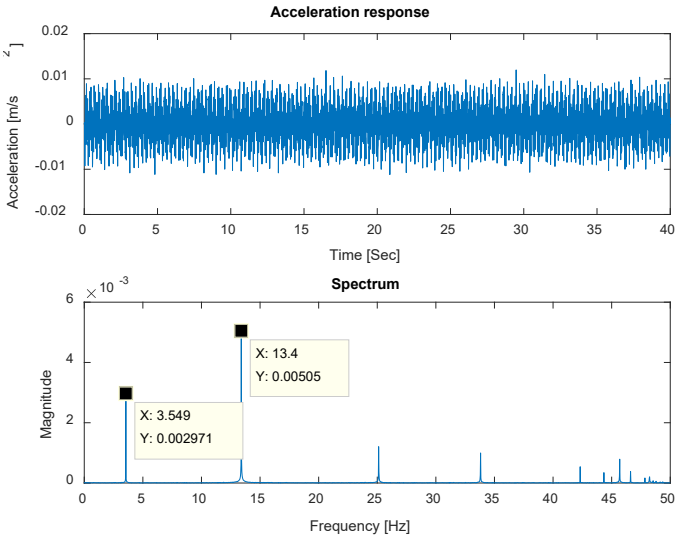

Figure 4 Bridge response and spectrum

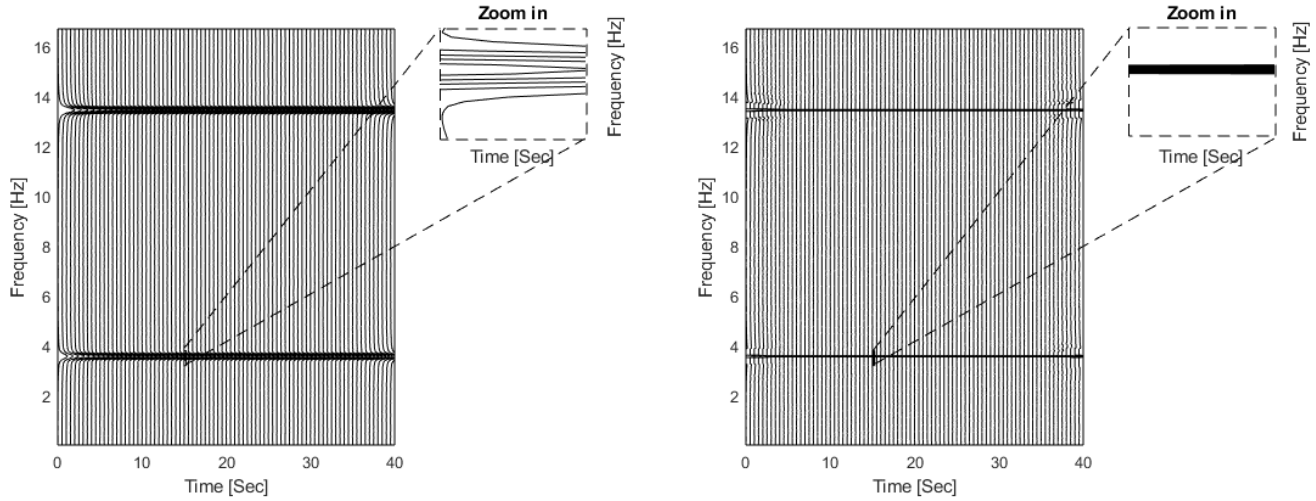

(a) TFR by STFT (b) TFR by SET

Figure 5 Time-frequency representation of the bridge response

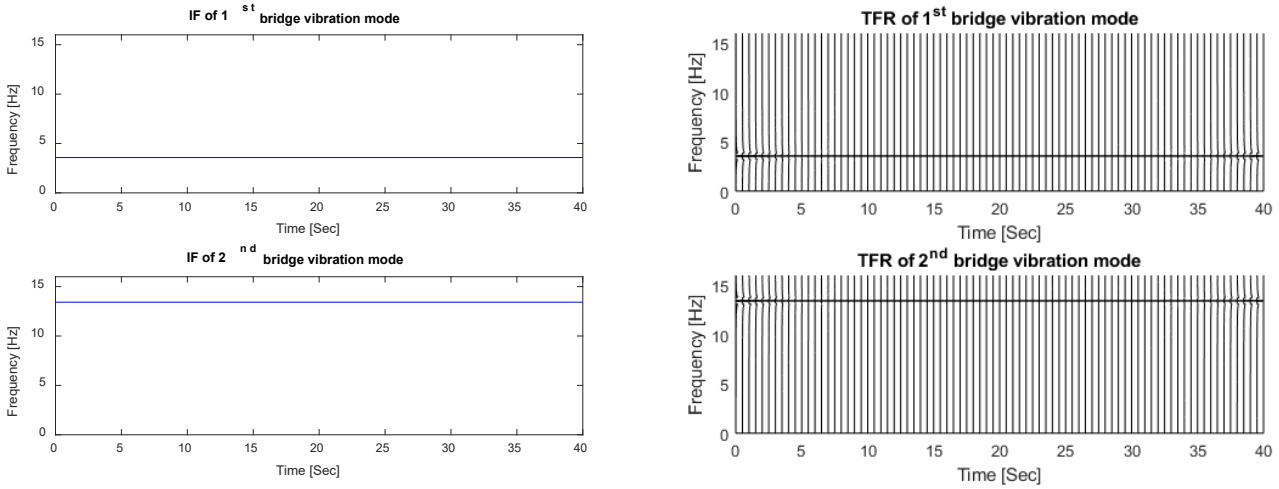

(a) IF of response components (b) TFR of response components

Figure 6 IF and TFR of bridge response components

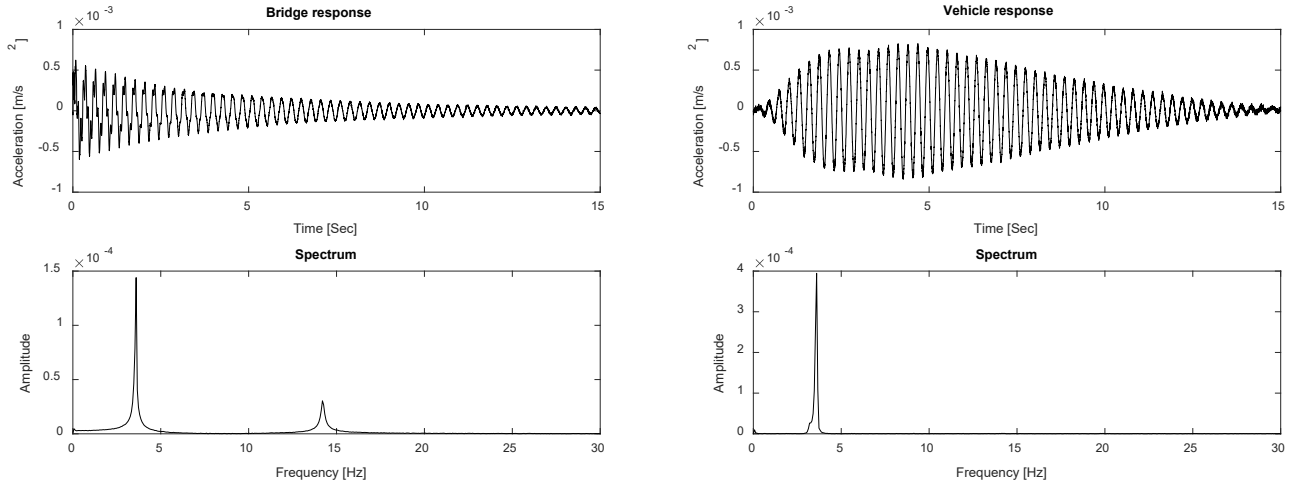

(a) Bridge response and spectrum (b) Vehicle respose and spectrum

Figure 7 Vehicle and bridge responses in the VBI system and their spectra

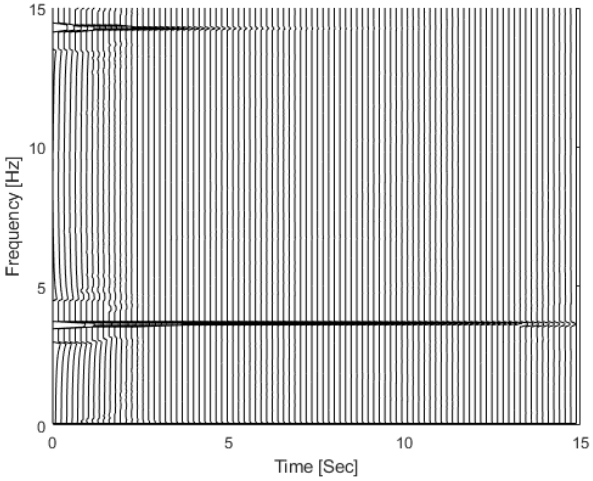

(a) TFR of bridge response

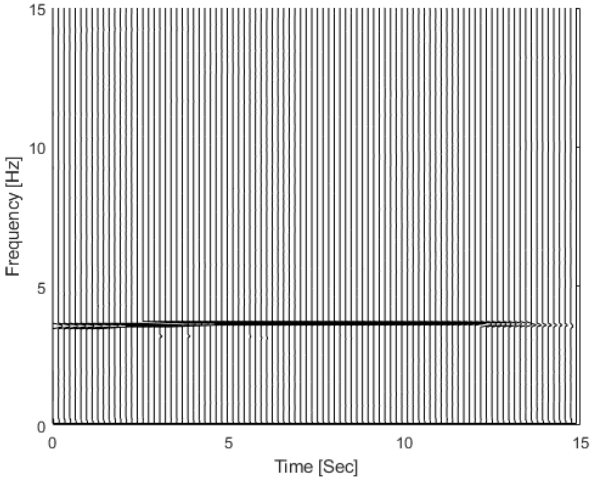

(b) TFR of vehicle response

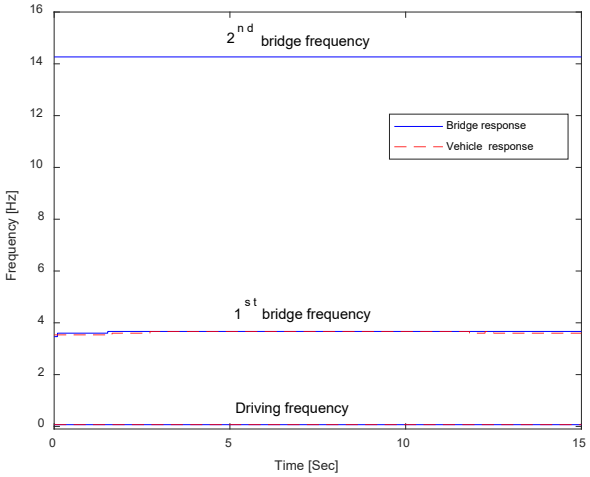

(c) IFs of the response components

Figure 8 TFR of the bridge and vehicle responses by SET

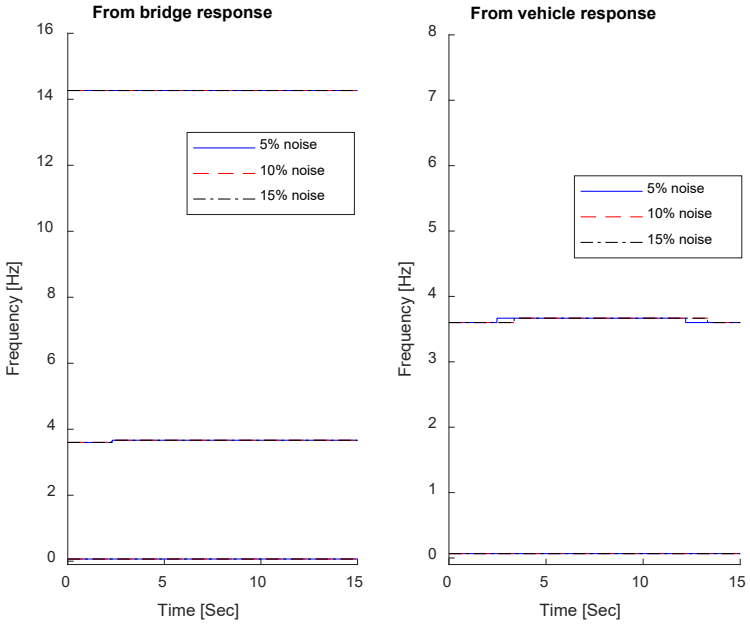

Figure 9. IFs of vehicle and bridge responses

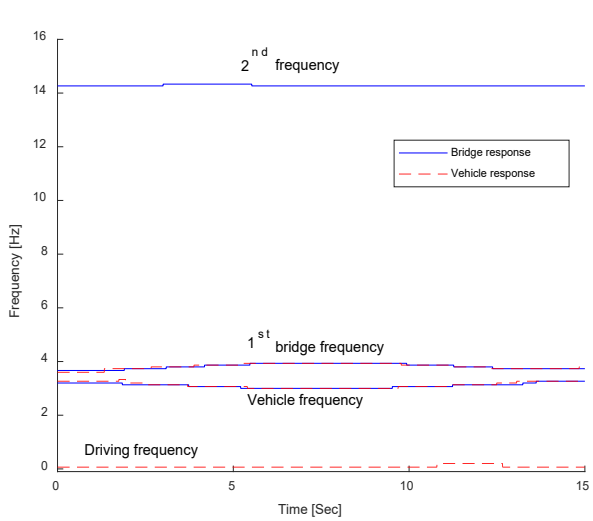

(a) TFR of bridge and vehicle response

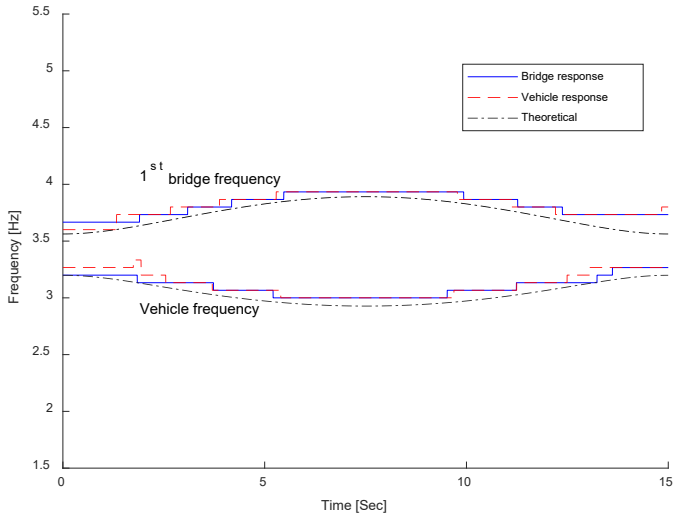

(b) Zoom in and compared with the theoretical values

Figure 10 TFR of the bridge and vehicle responses by SET for Vehicle2

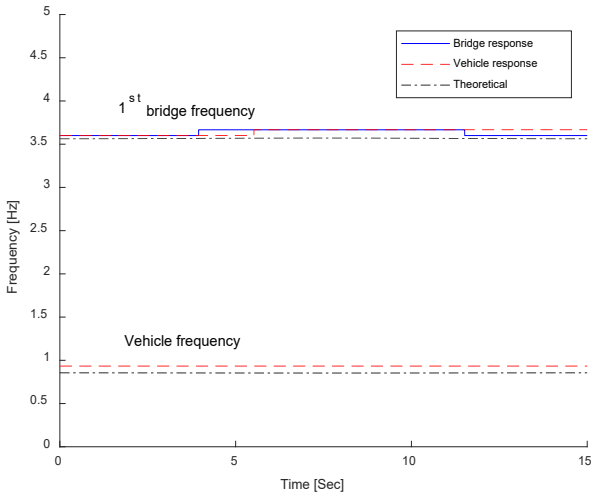

(a) Vehicle 3

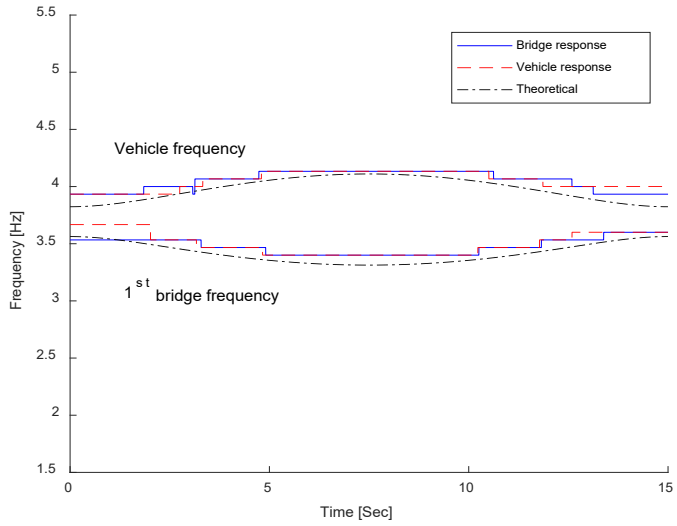

(b) Vehicle 4

Figure 11 TFR of the bridge and vehicle responses by SET for Vehicle 3 and 4

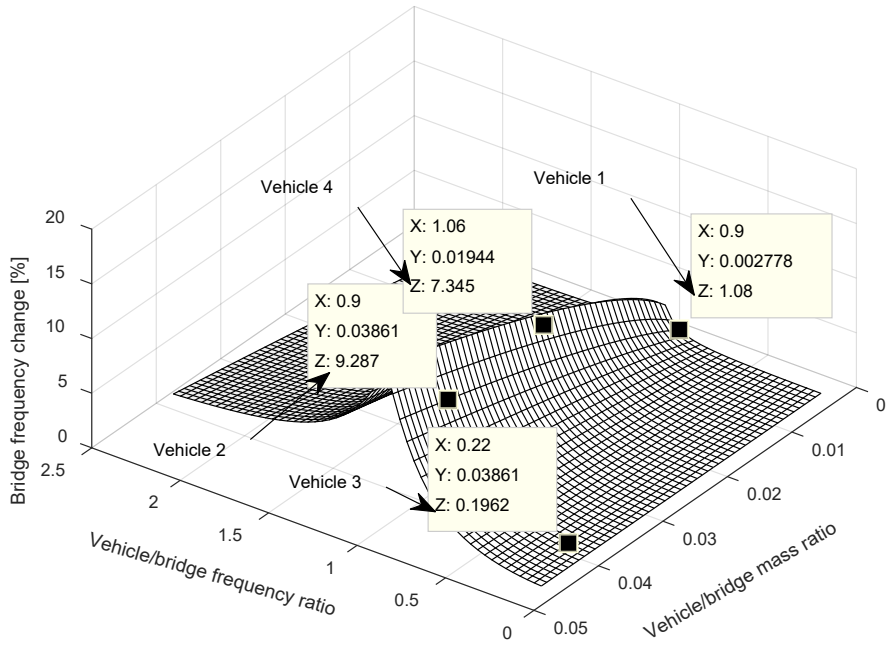

(a) Bridge frequency change

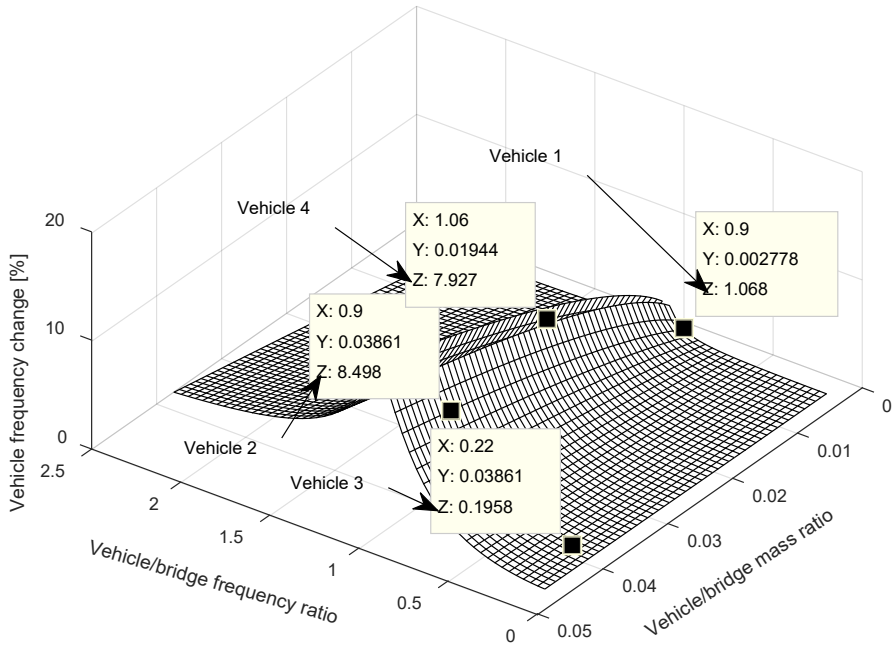

(b) Vehicle frequency change

Figure 12 Maximum frequency changes in relation to vehicle properties

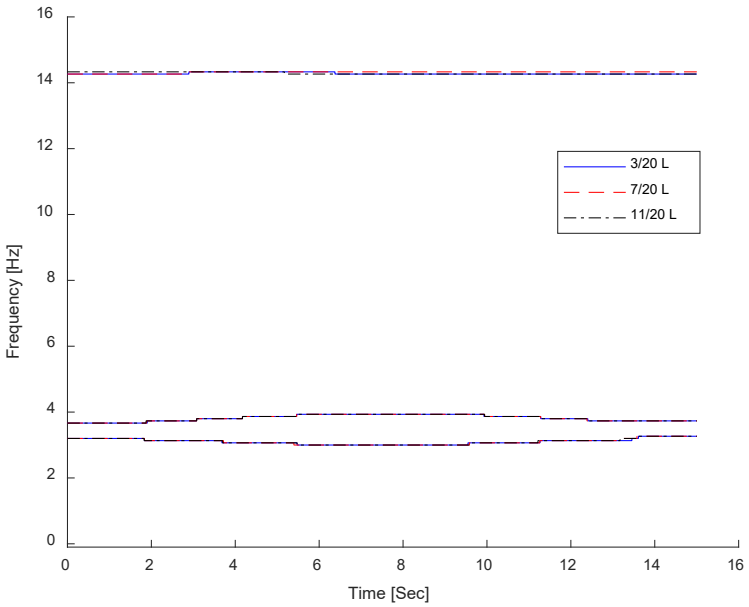

Figure 13. IF of vertical acceleration response measured at different points on bridge

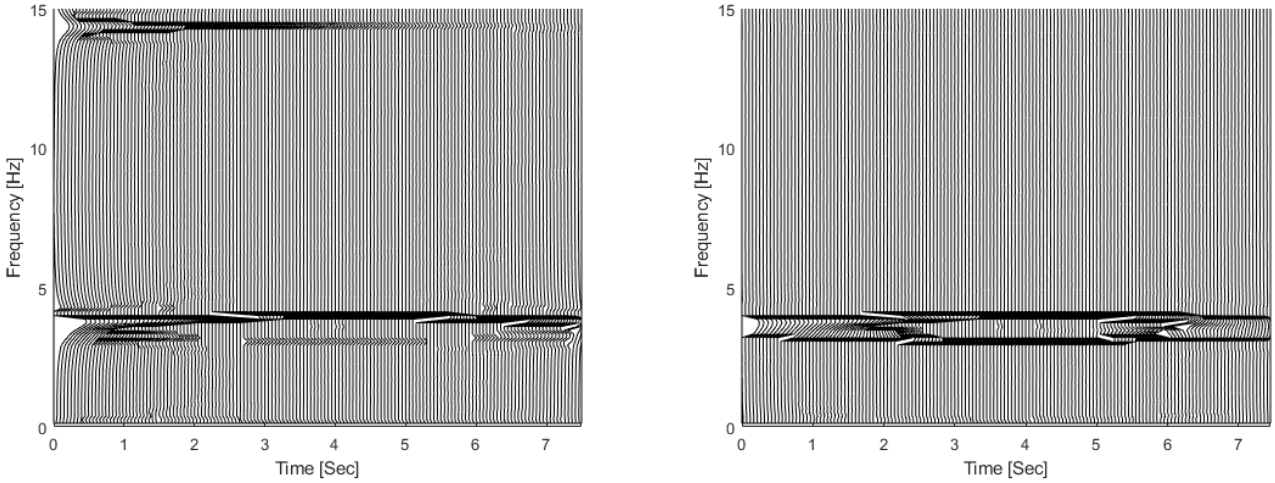

(a) TFR of bridge response (b) TFR of vehicle response

Figure 14 TFR of the bridge and vehicle responses by SET for Vehicle 2 when speed is 4m/s

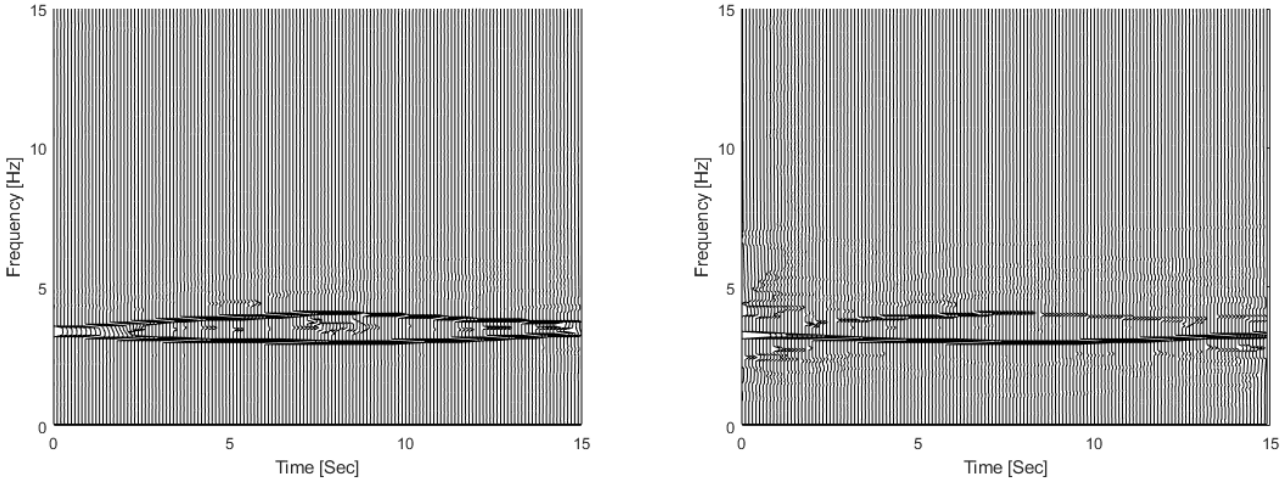

(a) TFR of bridge response (b) TFR of vehicle response

Figure 15 Time-frequency representation by SET considering Class A surface roughness

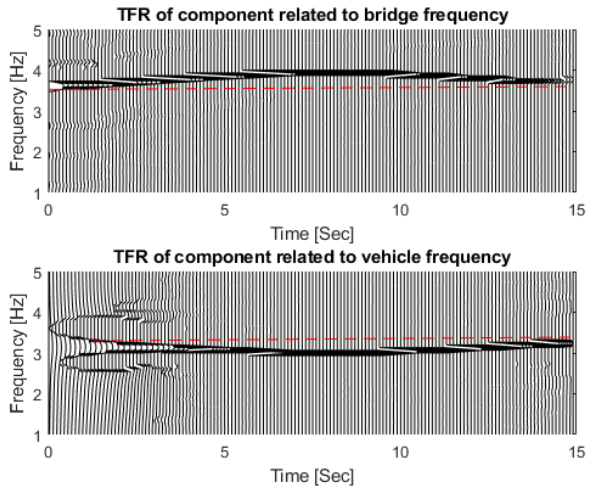

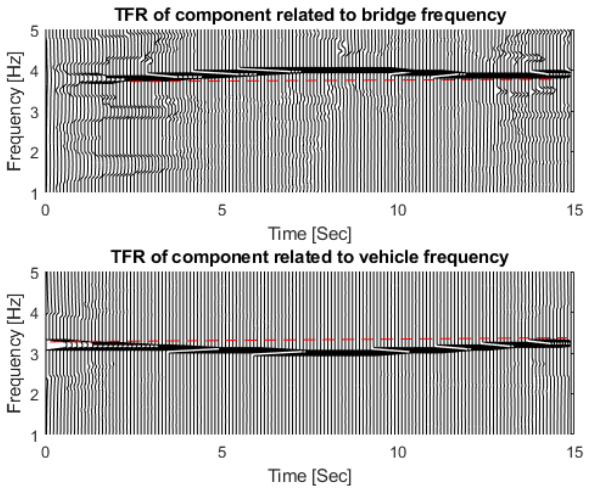

(a) TFR of components for smooth bridge surface (b) TFR of components for Class A surface roughness

Figure 16 TFR of extracted modes related to bridge and vehicle frequencies from vehicle responses

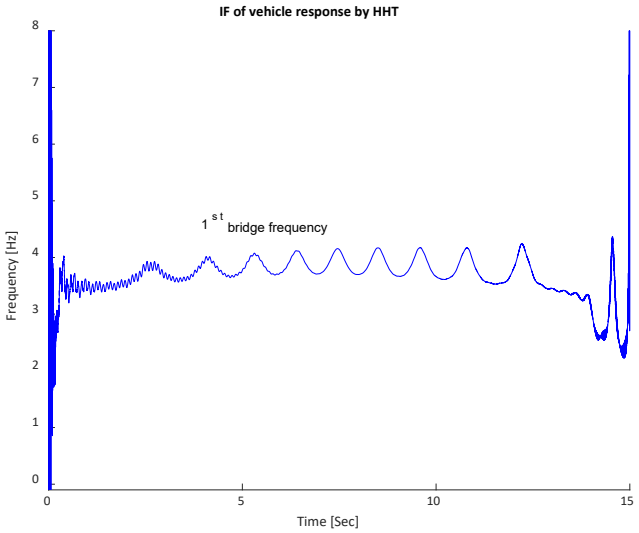

(a) Identified IF of vehicle response by HHT

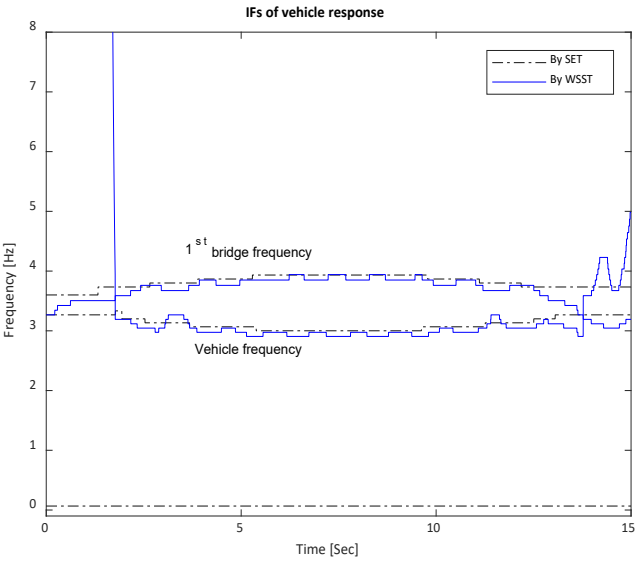

(b) Identified Ifs of vehicle response by SET and WSST

Figure 17 Comparison of three techniques for the identification of IFs of vehicle response

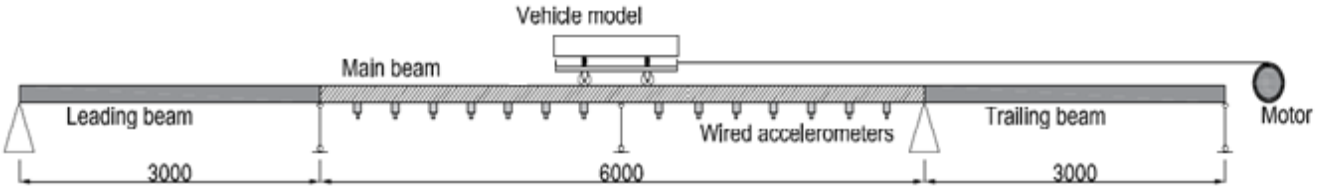

Figure 18 Schematic diagram of the VBI test system in the lab

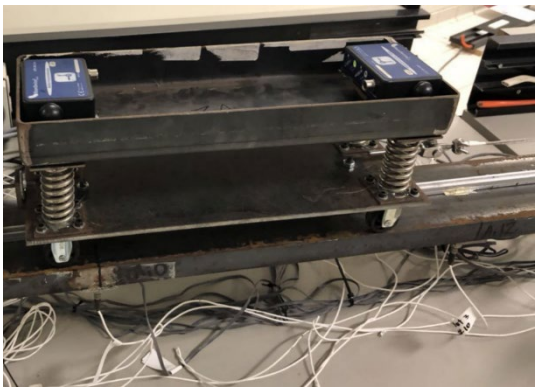

Figure 19 Instrumentation on the vehicle models with wireless sensors

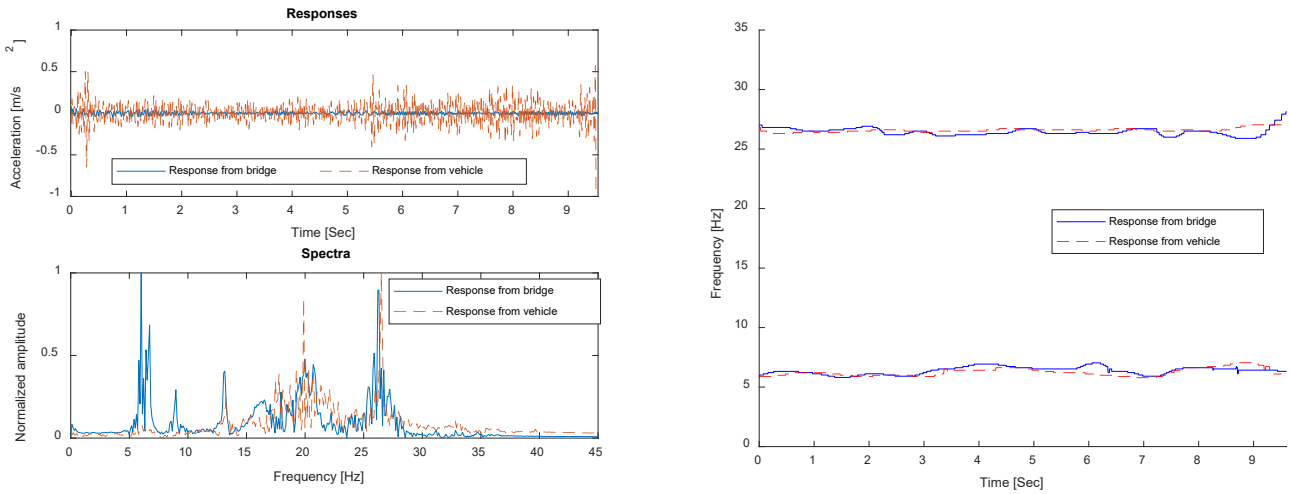

(a) Measured responses and spectrum (b) IFs of the signals

Figure 20 Measured responses

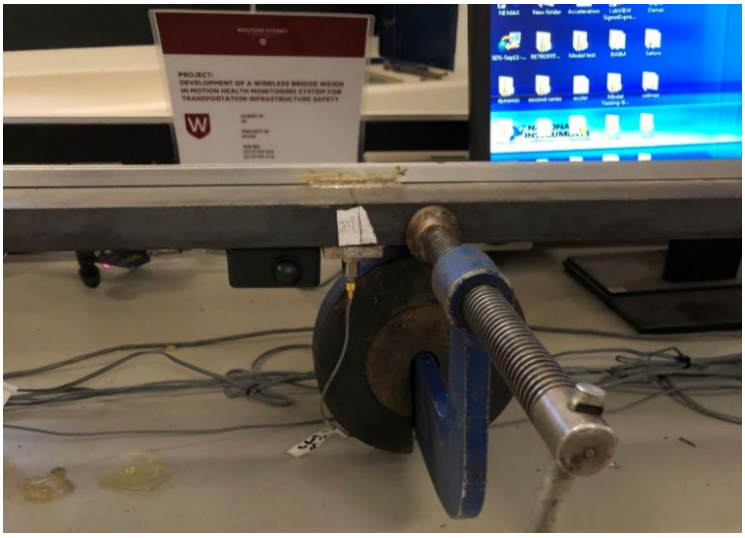

Figure 21 Adding mass to the beam model

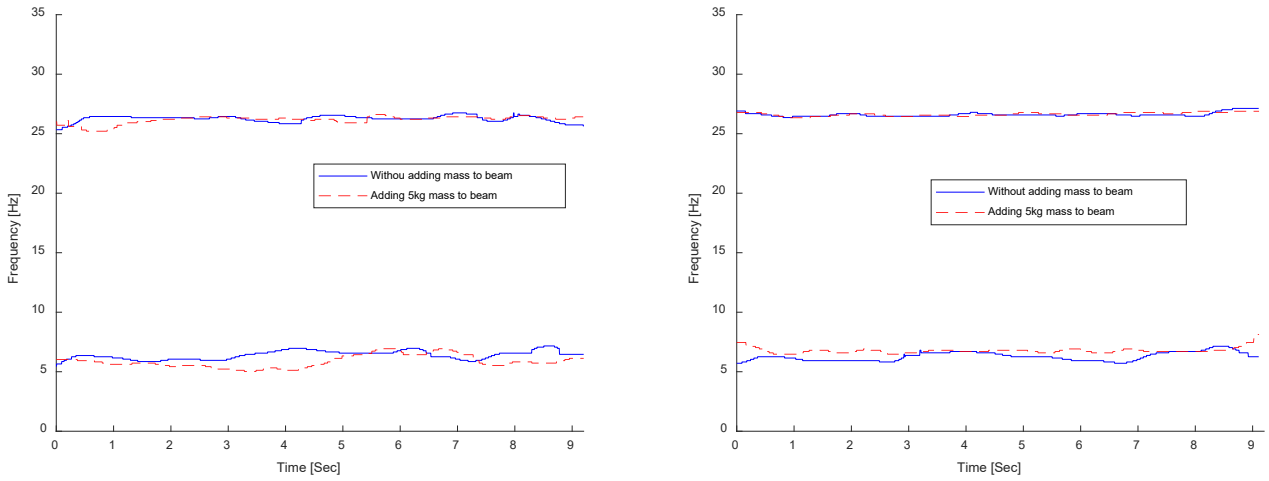

(a) Bridge response (b) Vehicle response

Figure 22 Instantaneous frequency

(a) The cable-stayed bridge

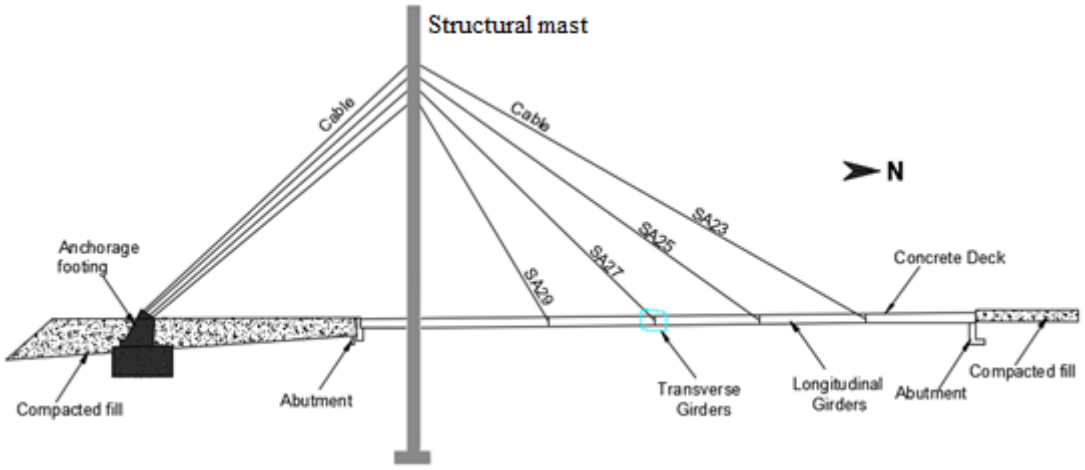

(b) The cable-stayed bridge

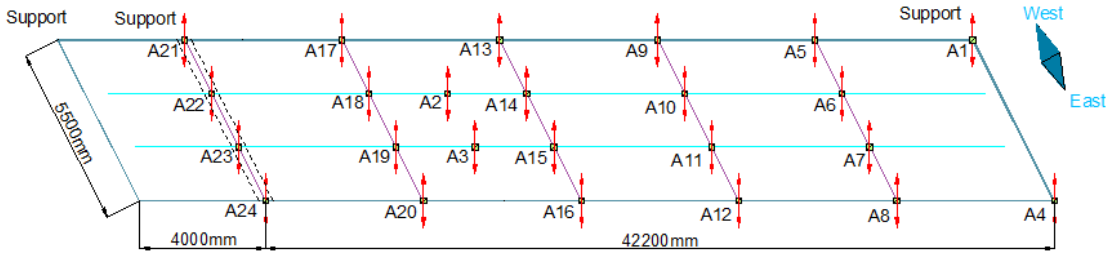

(c) Sensor location

Figure 23 Long-term monitoring of a cable-stayed bridge

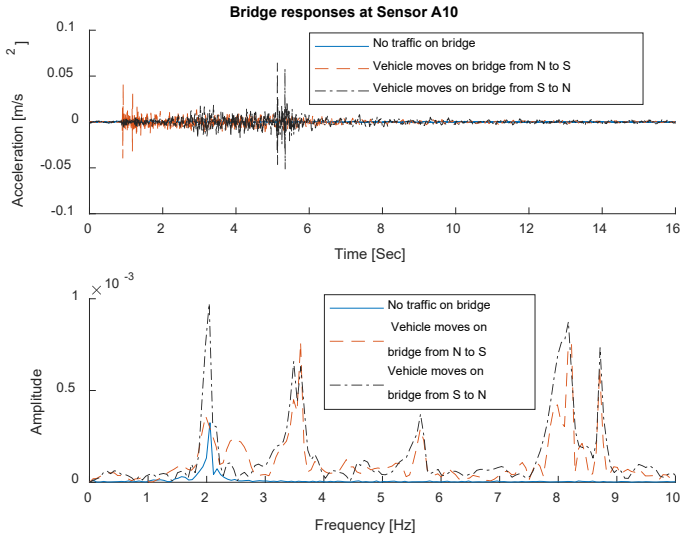

Figure 24 Acceleration responses and response spectra under different traffic conditions

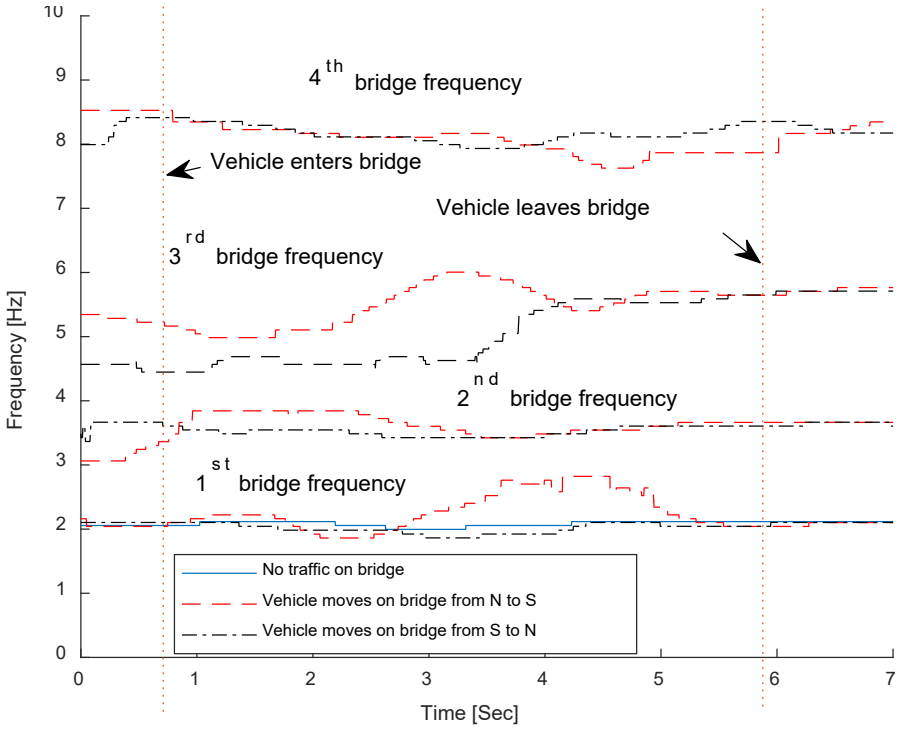

Figure 25 TF trajectories of responses for different traffic conditions

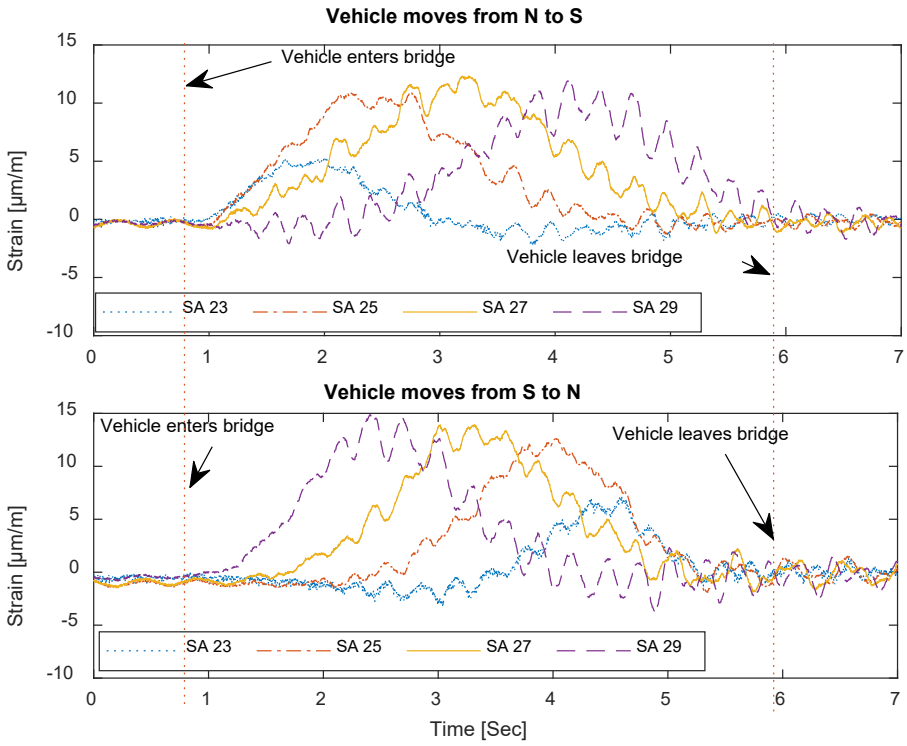

Figure 26 Strain measurements on the cables when vehicle moves in different directions

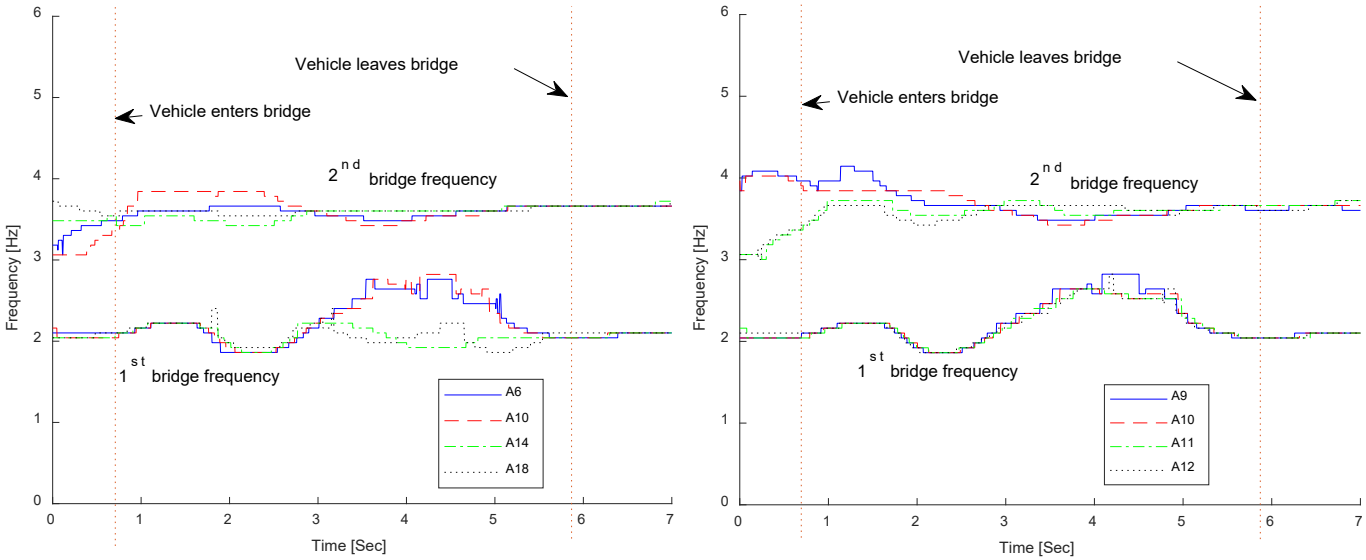

(a) Sensors along longitudinal direction (b) Sensors along transverse direction

Figure 27 IFs from responses at different locations